Article

Reversible Molecular Switching of Ruthenium Bis(bipyridyl) Groups Bonded to Oligothiophenes: Effect on Electrochemical and Spectroscopic Properties

Carolyn Moorlag, Michael O. Wolf, Cornelia Bohne, and Brian O. Patrick

J. Am. Chem. Soc., **2005**, 127 (17), 6382-6393• DOI: 10.1021/ja043573a • Publication Date (Web): 12 April 2005

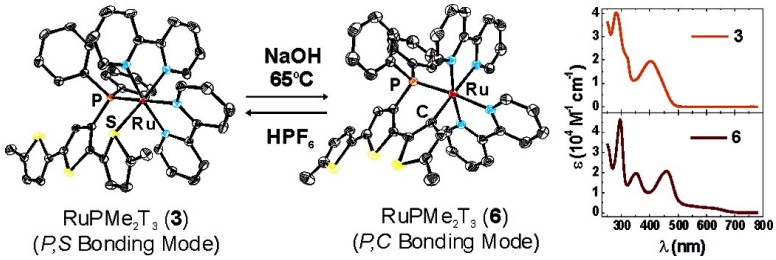

More About This Article

Additional resources and features associated with this article are available within the HTML version:

- Supporting Information
- Links to the 2 articles that cite this article, as of the time of this article download
- Access to high resolution figures
- Links to articles and content related to this article
- Copyright permission to reproduce figures and/or text from this article

View the Full Text HTML

J|A|C|S
ARTICLES
Published on Web 04/12/2005

Reversible Molecular Switching of Ruthenium Bis(bipyridyl) Groups Bonded to Oligothiophenes: Effect on Electrochemical and Spectroscopic Properties

Carolyn Moorlag,[†] Michael O. Wolf,*,[†] Cornelia Bohne,[‡] and Brian O. Patrick[†]

Contribution from the Department of Chemistry, The University of British Columbia, Vancouver, British Columbia, V6T 1Z1, Canada, and Department of Chemistry, The University of Victoria, P.O. Box 3065, Victoria, British Columbia, V8W 3V6, Canada

Received October 22, 2004; E-mail: mwolf@chem.ubc.ca

Abstract: We report the preparation of complexes in which ruthenium(II) bis(bipyridyl) groups are coordinated to oligothiophenes via a diphenylphosphine linker and a thienyl sulfur (*P*,*S* bonding) to give $[Ru(bpy)_2PT_3$-*P*,*S*$](PF_6)_2$ (bpy = 2,2′-bipyridyl, PT_3 = 3′-(diphenylphosphino)-2,2′:5′,2″-terthiophene), $[Ru(bpy)_2PMeT_3$-*P*,*S*$](PF_6)_2$ ($PMeT_3$ = 3′-(diphenylphosphino)-5-methyl-2,2′:5′,2″-terthiophene), $[Ru(bpy)_2PMe_2T_3$-*P*,*S*$](PF_6)_2$ (PMe_2T_3 = 5,5″-dimethyl-3′-(diphenylphosphino)-2,2′:5′,2″-terthiophene), and $[Ru(bpy)_2PDo_2T_5$-*P*,*S*$](PF_6)_2$ (PDo_2T_5 = 3,3‴-didodecyl-3″-diphenylphosphino-2,2′:5′,2″:5″,2‴:5‴,2⁗-pentathiophene). These complexes react with base, resulting in the complexes $[Ru(bpy)_2PT_3$-*P*,*C*$]PF_6$, $[Ru(bpy)_2PMeT_3$-*P*,*C*$]PF_6$, $[Ru(bpy)_2PMe_2T_3$-*P*,*C*$]PF_6$, and $[Ru(bpy)_2PDo_2T_5$-*P*,*C*$]PF_6$, where the thienyl carbon is bonded to ruthenium (*P*,*C* bonding). The *P*,*C* complexes revert back to the *P*,*S* bonding mode by reaction with acid; therefore, metal−thienyl bonding is reversibly switchable. The effect of interaction of the metal groups in the different bonding modes with the thienyl backbone is reflected by changes in alignment of the thienyl rings in the solid-state structures of the complexes, the redox potentials, and the $\pi \rightarrow \pi^*$ transitions in solution. Methyl substituents attached to the terthiophene groups allow observation of the effect of these substituents on the conformational and electronic properties and aid in assignments of the electrochemical data. The PT_n ligands bound in *P*,*S* and *P*,*C* bonding modes also alter the electrochemical and spectroscopic properties of the ruthenium bis(bipyridyl) group. Both bonding modes result in quenching of the oligothiophene luminescence. Weak, short-lived Ru → bipyridyl MLCT-based luminescence is observed for $[Ru(bpy)_2PDo_2T_5$-*P*,*S*$](PF_6)_2$, $[Ru(bpy)_2PT_3$-*P*,*C*$]PF_6$, $[Ru(bpy)_2PMeT_3$-*P*,*C*$]PF_6$, and $[Ru(bpy)_2PMe_2T_3$-*P*,*C*$]PF_6$, and no emission is observed for the alternate bonding mode of each complex.

Introduction

Polythiophenes are a class of π-conjugated organic polymers that have stimulated interest for application in new generations of electronic devices due to their many interesting physical properties such as electronic conductivity, electrochromism, and electroluminescence.[1−7] Functionalized polythiophenes, such as alkyl-[8−10] and halo-[11] substituted derivatives, have been synthesized to increase solubility, create centers for further functionalization, and alter the polymer properties. There has also been interest in modifying the backbone with metal groups to alter the physical, chemical, and electronic properties of polythiophene.[12−14] Electronic interactions between metals and polythiophenes may be modeled with shorter-chain oligothiophene complexes due to their ease of characterization and ability to be synthesized in pure form. Three methods of incorporating metals into oligo- or polythiophenes are as pendant groups attached via a ligand;[15,16] direct bonding to the backbone via thiophene,[17] bipyridyl[18−21] or bithiazole groups;[22] and metals inserted directly into the chain.[23−25] We are exploring the

[†] The University of British Columbia.
[‡] The University of Victoria.

(1) MacDiarmid, A. G. *Angew. Chem., Int. Ed.* **2001**, *40*, 2581−2590.
(2) Heeger, A. J. *Angew. Chem., Int. Ed.* **2001**, *40*, 2591−2611.
(3) Kraft, A.; Grimsdale, A. C.; Holmes, A. B. *Angew. Chem., Int. Ed.* **1998**, *37*, 402−428.
(4) Garnier, F.; Tourillon, G.; Gazard, M.; Dubios, J. C. *J. Electroanal. Chem.* **1983**, *148*, 299−303.
(5) Tourillon, G.; Garnier, F. *J. Phys. Chem.* **1983**, *87*, 2289−2292.
(6) Andersson, M. R.; Berggren, M.; Inganas, O.; Gustafsson, G.; Gustafsson-Carlberg, J. C.; Selse, D.; Hjertberg, T.; Wennerstrom, O. *Macromolecules* **1995**, *28*, 7525−7529.
(7) Berggren, M.; Inganas, O.; Gustafsson, G.; Rasmusson, J.; Andersson, M. R.; Hjertberg, T.; Wennerstrom, O. *Nature* **1994**, *372*, 444−446.
(8) Elsenbaumer, R. L.; Jen, K. Y.; Oboodi, R. *Synth. Met.* **1986**, *15*, 169−174.
(9) Loewe, R. S.; Ewbank, P. C.; Liu, J.; Zhai, L.; McCullough, R. D. *Macromolecules* **2001**, *34*, 4324−4333.
(10) Murray, K. A.; Moratti, S. C.; Baigent, D. R.; Greenham, N. C.; Pichler, K.; Holmes, A. B.; Friend, R. H. *Synth. Met.* **1995**, *69*, 395−396.
(11) Li, Y.; Vamvounis, G.; Yu, J.; Holdcroft, S. *Macromolecules* **2001**, *34*, 3130−3132.
(12) Peng, Z.; Gharavi, A. R.; Yu, L. *J. Am. Chem. Soc.* **1997**, *119*, 4622−4632.
(13) Walters, K. A.; Ley, K. D.; Cavalaheiro, C. S. P.; Miller, S. C.; Gosztola, D.; Wasielewski, M. R.; Bussandri, A. P.; van Willigen, H.; Schanze, K. S. *J. Am. Chem. Soc.* **2001**, *123*, 8329−8342.
(14) Wong, C. T.; Chen, W. K. *Adv. Mater.* **1999**, *11*, 455−459.
(15) Crayston, J. A.; Iraqi, A.; Morrison, J. J.; Walton, J. C. *Synth. Met.* **1997**, *84*, 441−442.
(16) Higgins, T. B.; Mirkin, C. A. *Chem. Mater.* **1998**, *10*, 1589−1595.
(17) Weinberger, D. A.; Higgins, T. B.; Mirkin, C. A.; Stern, C. L.; Liable-Sands, L. M.; Rheingold, A. L. *J. Am. Chem. Soc.* **2001**, *123*, 2503−2516.
(18) Zhu, S. S.; Swager, T. M. *Adv. Mater.* **1996**, *8*, 497−500.
(19) Zhu, S. S.; Kingsborough, R. P.; Swager, T. M. *J. Mater. Chem.* **1999**, *9*, 2123−2131.

10.1021/ja043573a CCC: $30.25

attachment of pendant metal groups that are also designed to bond to a thienyl group in the backbone.[26−28]

Thiophenes can bond to transition metals via various bonding modes, including η^1(S), η^2-, η^4-, or η^5-coordination[29] and metal−carbon bonding, most frequently at the thienyl α-position. Metals bonded to the thienyl group via a M−C bond may be formed by the reaction of a thienyl ring with metal fragments (cyclometalation)[30−32] or by conversion from η^1(S)-coordinated complexes, as has been demonstrated for rhenium− and ruthenium−thienyl complexes.[33,34] The effects of different bonding modes of a metal center to an oligothienyl chain on the properties of the conjugated oligomer are interesting. Ruthenium bis(bipyridyl) and ruthenium terpyridyl groups have been reported to coordinate to thienyltetrazine[35] and thienylbipyridine,[36,37] respectively, with the thiophene coordinated at the sulfur. Acid−base mediated reversible switching between sulfur coordination and a carbon bonding mode has been reported for a ruthenium thienylbipyridine complex.[38] In our approach, a pendant metal is covalently anchored through a phosphine group to an oligothiophene chain. The ruthenium bis(bipyridyl) (Ru(bpy)$_2$) group is selected due to the relative chemical inertness of the bpy spectator ligands, as well as the ability of some Ru(bpy)$_2$-containing complexes to undergo electron and energy transfer processes.[39] Two open coordination sites are available, allowing the possibility of bonding to a phosphino-oligothiophene via sulfur (*P*,*S*) or carbon (*P*,*C*) bidentate bonding modes. In a preliminary communication, we have reported the complexation of Ru(bpy)$_2$ to terthienyl units containing pendant diphenylphosphino groups[26] and demonstrated that coordination could be reversibly switched between *P*,*S* and *P*,*C* bonding modes.

In this article, we fully report the characterization of the model complexes [Ru(bpy)$_2$PT$_3$-*P*,*S*](PF$_6$)$_2$ (bpy = 2,2′-bipyridyl, PT$_3$ = 3′-(diphenylphosphino)-2,2′:5′,2″-terthiophene) (**1**), [Ru(bpy)$_2$PMeT$_3$-*P*,*S*](PF$_6$)$_2$ (PMeT$_3$ = 3′-(diphenylphosphino)-5-methyl-2,2′:5′,2″-terthiophene) (**2**), and [Ru(bpy)$_2$PMe$_2$T$_3$-*P*,*S*](PF$_6$)$_2$ (PMe$_2$T$_3$ = 5,5″-dimethyl-3′-(diphenylphosphino)-2,2′:5′,2″-terthiophene) and compare the electronic properties of these complexes with those of the carbon-bound complexes [Ru(bpy)$_2$PT$_3$-*P*,*C*]PF$_6$ (**4**), [Ru(bpy)$_2$PMeT$_3$-*P*,*C*]PF$_6$ (**5**), and [Ru(bpy)$_2$PMe$_2$T$_3$-*P*,*C*]PF$_6$ (**6**).

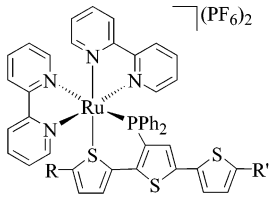

1 R = R' = H [Ru(bpy)$_2$PT$_3$-*P*,*S*](PF$_6$)$_2$
2 R = Me, R' = H [Ru(bpy)$_2$PMeT$_3$-*P*,*S*](PF$_6$)$_2$
3 R = R' = Me [Ru(bpy)$_2$PMe$_2$T$_3$-*P*,*S*](PF$_6$)$_2$

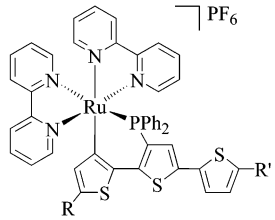

4 R = R' = H [Ru(bpy)$_2$PT$_3$-*P*,*C*]PF$_6$
5 R = Me, R' = H [Ru(bpy)$_2$PMeT$_3$-*P*,*C*]PF$_6$
6 R = R' = Me [Ru(bpy)$_2$PMe$_2$T$_3$-*P*,*C*]PF$_6$

The longer pentathiophene PDo$_2$T$_5$ (3,3‴″-didodecyl-3″-diphenylphosphino-2,2′:5′,2″:5″,2‴:5‴,2‴″-pentathiophene) (**7**) has been synthesized via selective coupling of dodecylthiophene groups to the terminal positions of tribromoterthiophene. The phosphine PDo$_2$T$_5$ was used to prepare [Ru(bpy)$_2$PDo$_2$T$_5$-*P*,*S*](PF$_6$)$_2$ (**8**), which can be reversibly switched to the carbon-bound complex [Ru(bpy)$_2$PDo$_2$T$_5$-*P*,*C*]PF$_6$ (**9**). The effect of the ruthenium bonding mode on the longer oligothiophene is compared with the results from the terthiophene complexes. The pentathiophene Do$_2$T$_5$ (3,3‴″-didodecyl-2,2′:5′,2″:5″,2‴:5‴,2‴″-pentathiophene) (**10**) was also synthesized for comparison to the ligand and complexes.

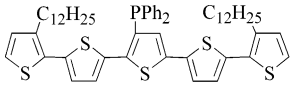

7 PDo$_2$T$_5$

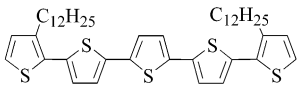

10 Do$_2$T$_5$

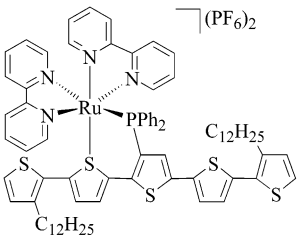

8 [Ru(bpy)$_2$PDo$_2$T$_5$-*P*,*S*](PF$_6$)$_2$

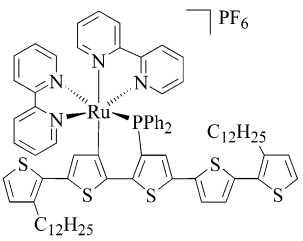

9 [Ru(bpy)$_2$PDo$_2$T$_5$-*P*,*C*]PF$_6$

Results

Synthesis and Structures of Complexes and Related Compounds. The preparation of the ligands PT$_3$, PMeT$_3$, and

(20) Trouillet, L.; De Nicola, A.; Guillerez, S. *Chem. Mater.* **2000**, *12*, 1611−1621.
(21) Walters, K. A.; Touillet, L.; Guillerez, S.; Schanze, K. S. *Inorg. Chem.* **2000**, *39*, 5496−5509.
(22) Wolf, M. O.; Wrighton, M. S. *Chem. Mater.* **1994**, *6*, 1526−1533.
(23) Zhu, Y.; Millet, D. B.; Wolf, M. O.; Rettig, S. J. *Organometallics* **1999**, *18*, 1930−1938.
(24) Fraysse, S.; Coudret, C.; Launay, J.-P. *J. Am. Chem. Soc.* **2003**, *125*, 5880−5888.
(25) Hjelm, J.; Constable, E. C.; Figgemeier, E.; Hagfeldt, A.; Handel, R.; Housecroft, C. E.; Mukhtar, E.; Schofield, E. *Chem. Commun.* **2002**, 284−285.
(26) Moorlag, C.; Clot, O.; Wolf, M. O.; Patrick, B. O. *Chem. Commun.* **2002**, 3028−3029.
(27) Clot, O.; Wolf, M. O.; Yap, G. P. A.; Patrick, B. O. *J. Chem. Soc., Dalton Trans.* **2000**, 2729−2737.
(28) Clot, O.; Wolf, M. O.; Patrick, B. O. *J. Am. Chem. Soc.* **2001**, *123*, 9963−9973.
(29) Angelici, R. J. *NATO ASI Ser., Ser. 3* **1998**, 89−127.
(30) Wang, R.; Groux, L. F.; Zargarian, D. *J. Organomet. Chem.* **2002**, *660*, 98−107.
(31) Morikita, T.; Hirano, M.; Sasaki, A.; Komiya, S. *Inorg. Chim. Acta* **1999**, *291*, 341−354.
(32) Bianchini, C.; Jimenez, M. V.; Meli, A.; Moneti, S.; Vizza, F. *J. Organomet. Chem.* **1995**, *504*, 27−31.
(33) Benson, J. W.; Angelici, R. J. *Inorg. Chem.* **1993**, *32*, 1871−1874.
(34) Robertson, M. J.; White, C. J.; Angelici, R. J. *J. Am. Chem. Soc.* **1994**, *116*, 5190−5195.
(35) Sarkar, B.; Kaim, W.; Klein, A.; Schwederski, B.; Fiedler, J.; Duboc-Toia, C.; Lahiri, G. K. *Inorg. Chem.* **2003**, *42*, 6172−6174.
(36) Constable, E. C.; Henney, R. P. G.; Tocher, D. A. *Chem. Commun.* **1989**, 913−914.
(37) Constable, E. C.; Henney, R. P. G.; Tocher, D. A. *J. Chem. Soc., Dalton Trans.* **1991**, 2335−2347.
(38) Constable, E. C.; Dunne, S. J.; Rees, D. G. F.; Schmitt, C. X. *Chem. Commun.* **1996**, 1169−1170.
(39) Kalyanasundaram, K. *Photochemistry of Polypyridine and Porphyrin Complexes*, 1st ed.; Academic Press: London, 1992.

Scheme 1

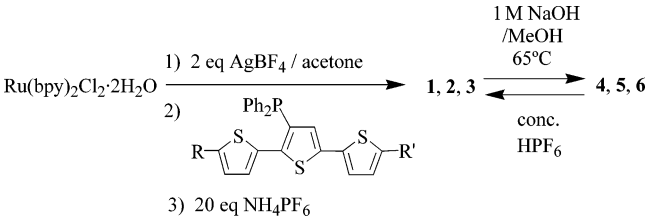

PMe_2T_3 has been previously reported.[27,28] Complexes **1**−**3** are prepared by reaction of $Ru(bpy)_2Cl_2 \cdot 2H_2O$ with $AgBF_4$ and complexation with the appropriate ligand. The products are metathesized to the PF_6 salts and recrystallized in ethanol−acetone to give air-stable complexes **1**−**3** in good yield (Scheme 1).

The solid-state structures of **1**[26] and **3** were established by X-ray crystallography of crystals grown from slow diffusion of hexanes into a solution of the complex in acetone. The structure of **3** is shown in Figure 1, and selected bond lengths and torsion angles are collected in Table 1. The ligands bind to Ru in a *P*,*S* bonding mode, with the metal coordinated to the S_1 thienyl ring in a η^1(S) fashion, resulting in the formation of a six-membered ring. We have observed this mode previously in other ruthenium and palladium complexes.[27,28] The Ru_1-S_1 bond lengths of **1** and **3** are 2.3640 and 2.3621 Å, which is within the observed range for other S-bound ruthenium−thiophene complexes. The plane of the bound thiophene is tilted from the Ru−S bond at angles of 58.3° (**1**) and 53.6° (**3**), which minimizes π-antibonding interactions between the thiophene and the metal.[40] Some π-antibonding overlap is indicated by S_1-C_{33} and S_1-C_{36} bonds for **1** and **3** (1.74−1.76 Å) that approach C−S single bond lengths[41] and are elongated compared with calculated bond lengths for terthiophene (1.7206 and 1.7351 Å, respectively).[42] The $S_1-C_{36}-C_{37}-S_2$ and $S_2-C_{40}-C_{41}-S_3$ torsion angles of **1** (147.02°, 146.0°) are close to the calculated torsion angles of terthiophene (147.6°),[42] while the corresponding torsion angles of **3** (150.71°, 165.48°) indicate increased coplanarity and therefore greater π-orbital overlap of adjacent thienyl rings. Plane-to-plane distances of 3.3−3.8 Å between aromatic rings in solid-state molecular structures are indicative of π-stacking.[43,44] There is evidence for weak π-stacking between the tilted S_1 thienyl and N_2 pyridyl rings of **1** (plane-to-plane distance between centroids = 3.708 Å) and **3** (3.675 Å) and the N_4 pyridyl and C_{21} phenyl rings of both **1** (3.777 Å) and **3** (3.580 Å). These intramolecular π-stackings could promote the preferential crystallization of the diastereomers observed in the crystal structures of **1** and **3**, in which the S_1 thienyl ring is tilted toward the N_2 pyridyl ring rather than toward the edge of the N_4 pyridyl ring. Single peaks are observed in the ^{31}P NMR spectra, also providing no evidence for different diastereomers in solution. Intermolecular π-stacking between rings is not observed for **1**. Figure 2 depicts the alignment in the crystal structure of **3**, where the offset intermolecular S_1 and S_3' thienyl rings are weakly π-stacked with a plane-to-plane distance between centroids of 3.947 Å. Sulfur atoms of stacked rings are aligned anti to one another.

P,*C* complexes **4**−**6** are prepared by reaction of the corresponding *P*,*S* complexes **1**−**3** with NaOH dissolved in methanol and heating to reflux (Scheme 1). Yields (50−85%) are higher than those that have been previously reported for reactions with NaOH in CH_3CN/H_2O (10−50%).[26] Switching of the bonding mode, essentially a deprotonation and cyclometalation reaction, does not proceed without heating. A color change from yellow to dark brown indicates the onset of the cyclometalation reaction. Analysis of crude samples of the *P*,*C* complexes indicates the presence of some oxidized ligand, which is removed by crystallization. The solid-state structures of **4**[26] and **6** (Figure 1, Table 1) were established by X-ray crystallography from crystals grown by slow diffusion of hexanes into a solution of the complex in acetone. The cyclometalated thienyl ring is tilted very little from the Ru−C bond, with tilt angles of 7.3° for **4** and 8.6° for **6**. The Ru_1-C_{35} bond lengths (2.076 and 2.095 Å) are longer than the calculated double bond length in $Ru{=}CH_2^+$ (1.88 Å),[45] but shorter than Ru−C single bonds reported for ruthenium bound to alkyl ligands (2.22 Å),[46,47] indicating that there is some double bond character. π-Antibonding overlap greater than that for the *P*,*S* complexes would be expected due to the end-on bonding mode and is indicated by elongated thienyl C−C double bonds, notably for the $C_{35}-C_{36}$ bond, which is elongated by 0.044 Å for **4** and by 0.040 Å for **6** compared to **1** and **3**. The $S_1-C_{36}-C_{37}-S_2$ torsion angles of **4** (10.7°) and **6** (19.7°) correspond to syn S_1 and S_2 thienyl rings, while the *P*,*S* complexes show an anti arrangement of these rings, and the *P*,*C* complexes show greater coplanarity between all three thienyl rings compared to the *P*,*S* complexes. Intramolecular π-stacking is observed between the adjacent N_4 pyridyl and C_{21} phenyl rings of **4** based on a plane-to-plane distance of 3.510 Å, while in **6** the corresponding distance is 3.901 Å. Intermolecular thienyl rings of **4** and **6** are separated by >4 Å.

Complete reversion of *P*,*C* complexes **4**−**6** to the *P*,*S* complexes occurs rapidly with the addition of HPF_6 or HCl at room temperature, concomitant with a color change from deep brown to bright yellow. Analysis by ^{31}P NMR spectroscopy indicates that this conversion occurs quantitatively with no side products.

The ligand PDo_2T_5 (**7**) is synthesized in three steps from 5,3′,5″-tribromo-2,2′:5′,2″-terthiophene (Scheme 2). Selective coupling at the terminal bromo substituents is carried out via palladium-catalyzed Kumada coupling[48] with the Grignard reagant 2-bromo-3-dodecylthienyl-magnesium bromide to give 3″-bromo-3,3‴-didodecyl-2,2′:5′,2″:5″,2‴:5‴,2⁗-pentathiophene in good yield. The use of $Pd(dppf)Cl_2$ as a catalyst rather than $Ni(dppp)Cl_2$ results in preferential reaction at the α-positions. Exceeding 2 equiv of the Grignard reagant results in the formation of the T-shaped 3″-(2-(3-dodecyl)thiophene)-3,3⁗-didodecyl-2,2′:5′,2″:5″,2‴:5‴,2⁗-pentathiophene as a side product. The phosphine PDo_2T_5 could not be prepared by

(40) Harris, S. *Polyhedron* **1997**, *16*, 3219−3233.
(41) Rozsondai, B.; Schultz, G.; Hargittai, I. *J. Mol. Struct.* **1981**, *70*, 309−310.
(42) DiCesare, N.; Belletete, M.; Marrano, C.; Leclerc, M.; Durocher, G. *J. Phys. Chem. A* **1998**, *102*, 5142−5149.
(43) Curtis, M. D.; Cao, J.; Kampf, J. W. *J. Am. Chem. Soc.* **2004**, *126*, 4318−4328.
(44) Yamamoto, T.; Komarudin, D.; Maruyama, T.; Arai, M.; Lee, B.-L.; Suganuma, H.; Asakawa, N.; Inoue, Y.; Kubota, K.; Sasaki, S.; Fukuda, T.; Matsuda, H. *J. Am. Chem. Soc.* **1998**, *120*, 2047−2058.
(45) Carter, E. A.; Goddard, W. A., III. *J. Am. Chem. Soc.* **1986**, *108*, 2180−2191.
(46) Watanabe, M.; Murata, K.; Ikariya, T. *J. Am. Chem. Soc.* **2003**, *125*, 7508−7509.
(47) Bibal, C.; Pink, M.; Smurnyy, Y. D.; Tomaszewski, J.; Caulton, K. G. *J. Am. Chem. Soc.* **2004**, *126*, 2312−2313.
(48) Nakanishi, H.; Sumi, N.; Aso, Y.; Otsubo, T. *J. Org. Chem.* **1998**, *63*, 8632−8633.

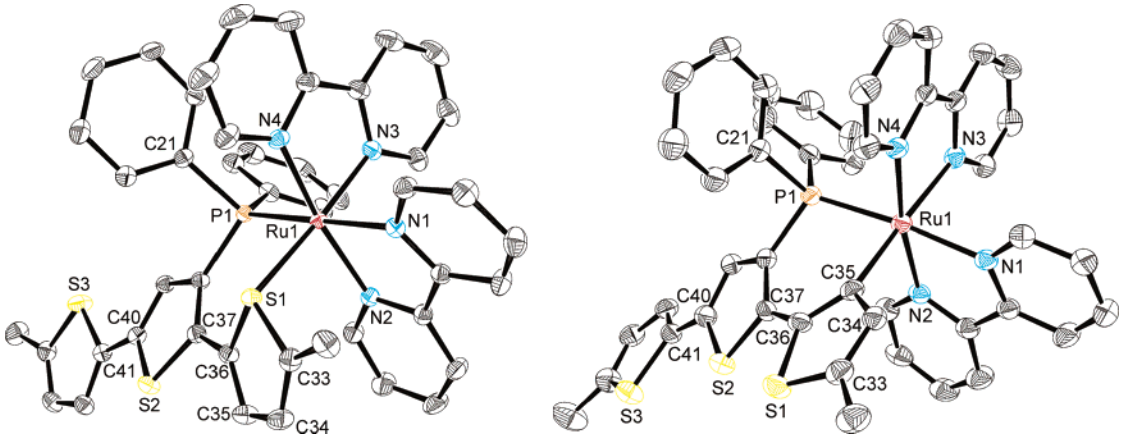

Figure 1. X-ray crystal structures of $[Ru(bpy)_2PMe_2T_3\text{-}P,S](PF_6)_2$ (**3**, left) and $[Ru(bpy)_2PMe_2T_3\text{-}P,C]PF_6$ (**6**, right). Hydrogen atoms are omitted for clarity, and thermal ellipsoids are drawn at 50% probability.

Table 1. Selected Bond Lengths and Angles for $[Ru(bpy)_2PMe_2T_3\text{-}P,S](PF_6)_2$ (**3**) and $[Ru(bpy)_2PMe_2T_3\text{-}P,C]PF_6$ (**6**)

3 bond length, Å		**6** bond length, Å	
Ru_1-S_1	2.3621(6)	Ru_1-C_{35}	2.095(2)
Ru_1-P_1	2.3397(6)	Ru_1-P_1	2.2954(7)
S_1-C_{33}	1.764(2)	S_1-C_{33}	1.734(3)
S_1-C_{36}	1.750(2)	S_1-C_{36}	1.758(2)
$C_{33}-C_{34}$	1.347(3)	$C_{33}-C_{34}$	1.370(4)
$C_{34}-C_{35}$	1.433(3)	$C_{34}-C_{35}$	1.450(3)
$C_{35}-C_{36}$	1.356(3)	$C_{35}-C_{36}$	1.398(3)
$C_{36}-C_{37}$	1.449(3)	$C_{36}-C_{37}$	1.448(4)
torsion angle, deg		torsion angle, deg	
$S_1-C_{36}-C_{37}-S_2$	150.71(12)	$S_1-C_{36}-C_{37}-S_2$	−19.7(3)
$S_2-C_{40}-C_{41}-S_3$	−165.48(12)	$S_2-C_{40}-C_{41}-S_3$	16.0(3)

bromo-lithium exchange followed by addition of PPh_2Cl due to low reactivity of the lithio anion. An alternative high-temperature copper-catalyzed halogen exchange reaction[49] is used to form 3,3‴′-didodecyl-3″-iodo-2,2′:5′,2″:5″,2‴:5‴,2⁗-pentathiophene in high yield, and subsequent palladium-catalyzed cross-coupling with diphenylphosphine[50] yields PDo_2T_5 (**7**). The overall yield of 87% for the two-step process is an improvement over reported yields for phosphino-oligothiophenes prepared via lithiation and addition of PPh_2Cl.[27,28]

Ruthenium bipyridyl complexes $[Ru(bpy)_2PDo_2T_5\text{-}P,S](PF_6)_2$ (**8**) and $[Ru(bpy)_2PDo_2T_5\text{-}P,C]PF_6$ (**9**) are synthesized by the same procedures as for the *P*,*S* and *P*,*C* terthiophene complexes (Scheme 3). Repeated crystallizations of **8** in ethanol containing minimal acetone produced brightly colored orange needle-shaped crystals for X-ray analysis. In the crystal structure of **8** (Figure 3), one $[PF_6]^-$ counterion is replaced with $[BF_4]^-$. Compared to **1** and **3**, the Ru−S bond is shorter (2.3578 Å, Table 2), and the tilt angle between the thiophene ring and the Ru−S bond (58.4°) is comparable. The S_2-C_5 (1.762 Å) and S_2-C_8 (1.745 Å) bonds are elongated 0.011−0.028 Å compared to the inner ring of terthiophene (1.7342 Å).[42] The torsion angle between the two bound thiophene rings (147.9°) is very close to the corresponding torsion angle for **1** and the expected torsion angles for pentathiophene.[51,52] The disorder of the S_4 and S_5 rings of **8** is similar to the disorder observed in the crystal structure of pentathiophene[53] but may also be due to the long dodecyl chains. Intramolecular π-stacking is observed between the N_4 pyridyl and C_{45} phenyl rings and between the S_2 thienyl and N_1 pyridyl rings, with interplanar distances of 3.520 and 3.671 Å, respectively. Similar to **1** and **3**, there is a preference for the diastereomeric arrangement of the S_2 thienyl ring as depicted that may be due to π-stacking within the molecule. Intermolecular π-stacking is not seen in the crystal structure, possibly due to the observed alignment of the dodecyl chains between the molecules.

$[Ru(bpy)_2PDo_2T_5\text{-}P,C]PF_6$ (**9**) is a very dark red solid of which crystals could not be obtained for X-ray analysis, likely due to disorder of the pentathienyl group or the dodecyl chains combined with a reduction in the number of counterions compared to **8**. Reversion to the *P*,*S* complex **8** proceeded as for **4**−**6**, with addition of acid to a dissolved sample resulting in a color change from deep red to bright orange. The reaction is quantitative, and the lack of side products is clear from the data shown in Figure 4.

3,3‴′-Didodecyl-2,2′:5′,2″:5″,2‴:5‴,2⁗-pentathiophene (**10**) is prepared in quantitative yield by exchange of 3,3‴′-didodecyl-3″-iodo-2,2′:5′,2″:5″,2‴:5‴,2⁗-pentathiophene with butyllithium followed by quenching with H_2O (Scheme 4). Because of the stability of the charged pentathiophene, the reaction of the anion with water is slow. The resulting dark yellow powder is susceptible to oxidation in air.

Cyclic Voltammetry. The cyclic voltammograms of **1**−**3** are displayed in Figure 5a. Addition of electron-donating methyl substituents lowers the oxidation potentials, and progressively lower irreversible ruthenium oxidation waves at 1.48, 1.44, and 1.41 V are observed (Table 3). The only prominent thienyl oxidation wave is a shoulder at 1.69 V for **3**. New return waves observed on the first and subsequent scans of **1** and **2** at 1.14 and 1.12 V could be due to oxidative electropolymerization or dimerization at the terthienyl α-positions. A new return wave is not observed for methyl-capped complex **3**. The first bipyridine reduction is irreversible for **1**, which could indicate interaction of the reduced bipyridyl group with the relatively electron-poor terthienyl group. Two reversible bipyridine reduc-

(49) Klapars, A.; Buchwald, S. L. *J. Am. Chem. Soc.* **2002**, *124*, 14844−14845.
(50) Herd, O.; Hessler, A.; Hingst, M.; Tepper, M.; Stelzer, O. *J. Organomet. Chem.* **1996**, *522*, 69−76.
(51) Becker, R. S.; de Melo, J. S.; Macanita, A. L.; Elisei, F. *J. Phys. Chem.* **1996**, *100*, 18683−18695.
(52) DiCesare, N.; Belletete, M.; Donat-Bouillud, A.; Leclerc, M.; Durocher, G. *J. Lumin.* **1999**, *81*, 111−125.
(53) Azumi, R.; Goto, M.; Honda, K.; Matsumoto, M. *J. Chem. Soc. Jpn.* **2003**, *76*, 1561−1567.

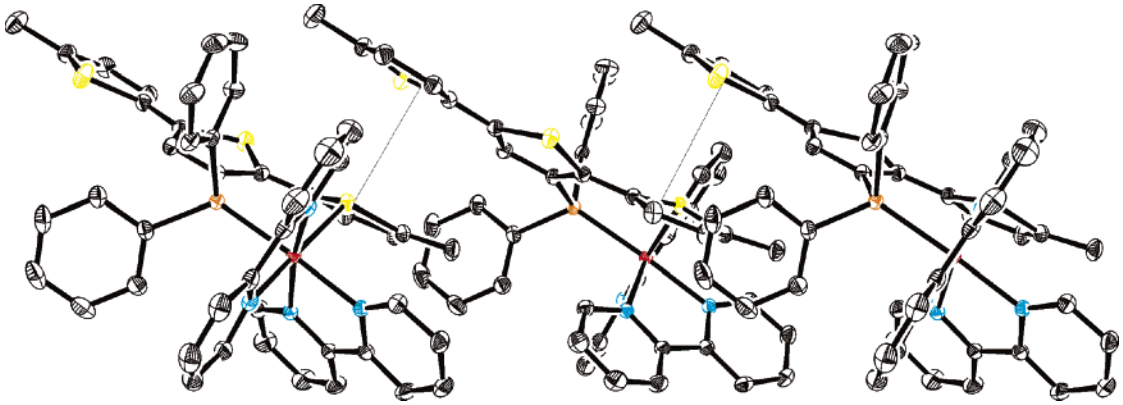

Figure 2. A portion of the unit cell of $[Ru(bpy)_2PMe_2T_3\text{-}P,S](PF_6)_2$ (**3**) viewed normal to the *010* plane. Lines are drawn between thienyl groups that are stacked relative to one other. Hydrogen atoms, $[PF_6]^-$, and occluded solvent have all been removed for clarity, and thermal ellipsoids are drawn at 50% probability.

Scheme 2

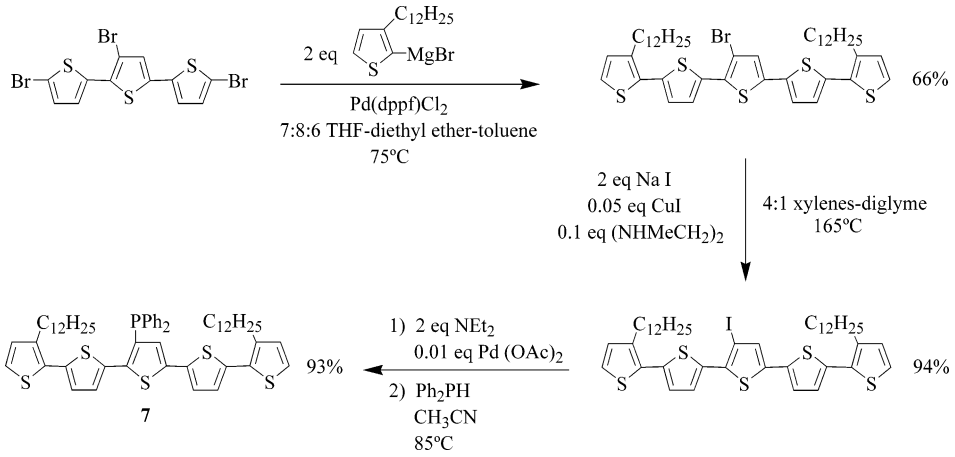

Scheme 3

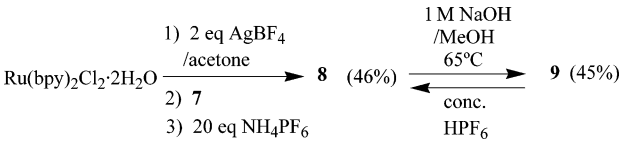

tions are observed at −1.24 and −1.46 V for **2** and **3**; the reversibility is possibly due to donation of electron density from the methyl substituents. Terthienyl reduction waves are observed at −1.79 and −1.81 V for **2** and **3**, respectively, with a negative shift in potential with addition of a methyl substituent.

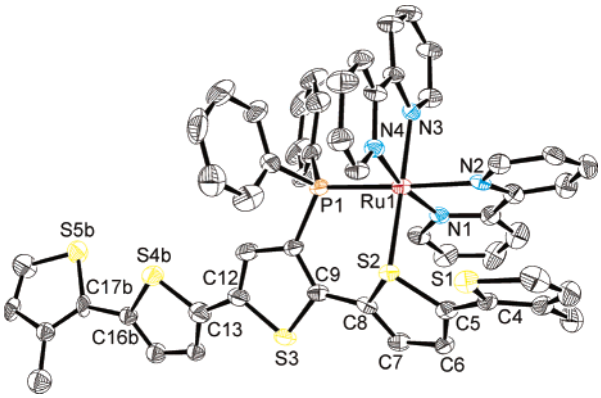

Figure 3. X-ray crystal structure of $[Ru(bpy)_2PDo_2T_5\text{-}P,S](PF_6)_2$ (**8**) (conformation B). Only the first carbon atoms of the dodecyl chains are included, and the remaining carbon atoms of the chains and all hydrogen atoms are omitted for clarity. Thermal ellipsoids are shown at 50% probability.

Table 2. Selected Bond Lengths and Angles for $[Ru(bpy)_2PDo_2T_5\text{-}P,S](PF_6)_2$ (**8**)

bond length, Å			
Ru_1-S_2	2.3578(14)	C_6-C_7	1.433(8)
Ru_1-P_1	2.3404(17)	C_7-C_8	1.353(8)
S_2-C_8	1.745(6)	C_8-C_9	1.469(8)
C_5-C_6	1.358(8)	S_2-C_5	1.762(6)
torsion angle, deg			
$S_1-C_4-C_5-S_2$	32.0(6)	$S_3-C_{12}-C_{13}-S_{4b}$	177.1(4)
$S_2-C_8-C_9-S_3$	−147.9(4)	$S_{4a}-C_{16a}-C_{17a}-S_{5a}$	154.8(9)
$S_3-C_{12}-C_{13}-S_{4a}$	127.9(5)	$S_{4b}-C_{16b}-C_{17b}-S_{5b}$	50.2(19)

The cyclic voltammograms of the *P,C* complexes **4**, **5**, and **6** (Figure 5b) display $Ru^{II/III}$ oxidations (0.49−0.57 V), terthienyl oxidations (0.96−1.11 V), and two bipyridyl reductions (1.53−1.55, 1.78 V). Ruthenium oxidations decrease ~0.9 V and terthienyl oxidations decrease >0.6 V compared to the *P,S* complexes, while the bipyridyl reductions are less affected by conversion to the *P,C* bonding mode. Assignments of the oxidation and reduction potentials of the *P,C* complexes are substantiated by addition of two methyl substituents having an effect on the thienyl oxidation potential (0.15 V decrease) greater than that on the ruthenium oxidation potential (0.08 V decrease), and almost no effect on bipyridyl reduction potentials.

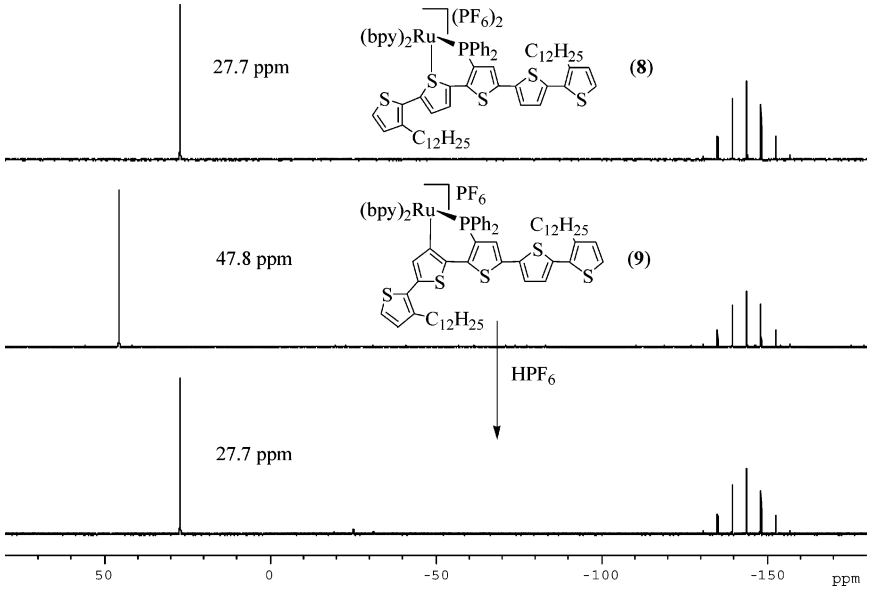

Figure 4. ^{31}P NMR spectra of [Ru(bpy)$_2$PDo$_2$T$_5$-*P*,*S*](PF$_6$)$_2$ (**8**, top) and [Ru(bpy)$_2$PDo$_2$T$_5$-*P*,*C*]PF$_6$ (**9**, middle). Addition of HPF$_6$ (concd) to a solution of **9** results in reversion to [Ru(bpy)$_2$PDo$_2$T$_5$-*P*,*S*](PF$_6$)$_2$ (bottom) as is observed by the reappearance of the peak at δ 27.7 and a dramatic color change from deep red to bright orange.

Scheme 4

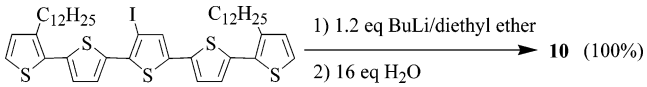

Cyclic voltammetry was performed on PDo$_2$T$_5$ (**7**), complexes [Ru(bpy)$_2$PDo$_2$T$_5$-*P*,*S*](PF$_6$)$_2$ (**8**) and [Ru(bpy)$_2$PDo$_2$T$_5$-*P*,*C*]PF$_6$ (**9**), and Do$_2$T$_5$ (**10**). Two irreversible oxidation waves are observed for **7** that are more positive than the first and second

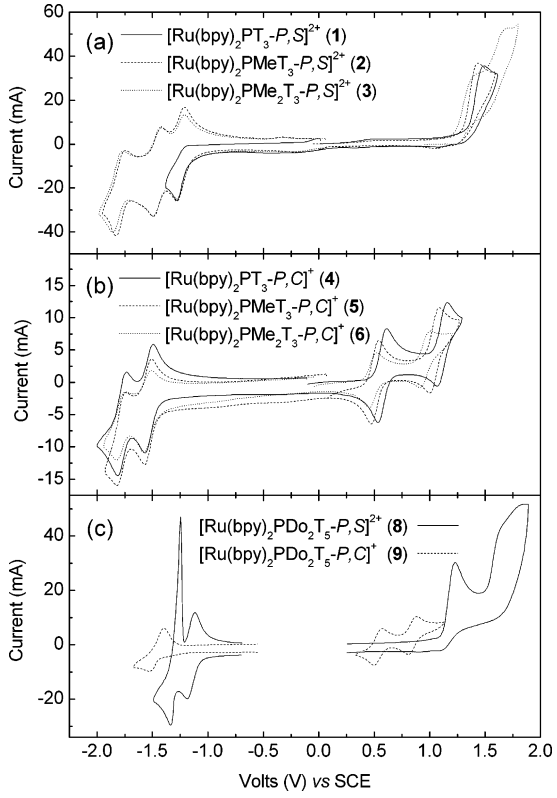

Figure 5. Cyclic voltammetry of (a) **1**−**3** (b) **4**−**6**, and (c) **8**−**9** in CH$_3$CN containing 0.1 M [(*n*-Bu)$_4$N]PF$_6$, scan rate = 100 mV/s. All complexes are PF$_6$ salts at 4.0 × 10^{-3} M concentrations.

Table 3. Cyclic Voltammetry Data[a]

compound	$E_{1/2,ox}$ ± 0.01 V	$E_{1/2,red}$ ± 0.01 V
[Ru(bpy)$_2$PT$_3$-*P*,*S*]$^{2+}$ (**1**)	+1.48[b] (Ru$^{II/III}$)	−1.28[b] (bpy$^{0/-}$)
[Ru(bpy)$_2$PMeT$_3$-*P*,*S*]$^{2+}$ (**2**)	+1.44[b] (Ru$^{II/III}$)	−1.24 (bpy$^{0/-}$)
		−1.46 (bpy$^{-/2-}$)
		−1.79 (PMeT$_3^{0/-}$)
[Ru(bpy)$_2$PMe$_2$T$_3$-*P*,*S*]$^{2+}$ (**3**)	+1.41(sh)[b,d] (Ru$^{II/III}$)	−1.24 (bpy$^{0/-}$)
	+1.69(sh)[b,d] (PMe$_2$T$_3^{0/+}$)	−1.46 (bpy$^{-/2-}$)
		−1.81 (PMe$_2$T$_3^{0/-}$)
[Ru(bpy)$_2$PT$_3$-*P*,*C*]$^+$ (**4**)	+0.57 (Ru$^{II/III}$)	−1.53 (bpy$^{0/-}$)
	+1.11 (PT$_3^{0/+}$)	−1.78 (bpy$^{-/2-}$)
[Ru(bpy)$_2$PMeT$_3$-*P*,*C*]$^+$ (**5**)	+0.51 (Ru$^{II/III}$)	−1.54 (bpy$^{0/-}$)
	+1.04 (PMeT$_3^{0/+}$)	−1.78 (bpy$^{-/2-}$)
[Ru(bpy)$_2$PMe$_2$T$_3$-*P*,*C*]$^+$ (**6**)	+0.49 (Ru$^{II/III}$)	−1.55 (bpy$^{0/-}$)
	+0.96 (PMe$_2$T$_3^{0/+}$)	−1.78 (bpy$^{-/2-}$)
PDo$_2$T$_5$ (**7**)	+0.99 (PDo$_2$T$_5^{0/+}$)	
	+1.37[b] (PDo$_2$T$_5^{+/2+}$)	
[Ru(bpy)$_2$PDo$_2$T$_5$-*P*,*S*]$^{2+}$ (**8**)	+1.21[b] (Ru$^{II/III}$)	−1.22 (bpy$^{0/-}$)
	+1.71(sh)[b,d] (PDo$_2$T$_5^{0/+}$)	−1.36 (bpy$^{-/2-}$)
[Ru(bpy)$_2$PDo$_2$T$_5$-*P*,*C*]$^+$ (**9**)	+0.49 (Ru$^{II/III}$)	−1.52 (bpy$^{0/-}$)
	+0.80 (PDo$_2$T$_5^{0/+}$)	−1.83 (bpy$^{-/2-}$)
	+1.46 (PDo$_2$T$_5^{+/2+}$)	
Do$_2$T$_5$ (**10**)[c]	+0.82 (Do$_2$T$_5^{0/+}$)	
	+1.07 (Do$_2$T$_5^{+/2+}$)	

[a] Measurements carried out in CH$_3$CN/0.1 M [(*n*-Bu)$_4$N]PF$_6$ solution with a Pt working electrode, Pt counter electrode, and a Ag wire quasi reference at 20 °C. Potentials are referenced to a decamethylferrocene standard and reported in volts vs SCE. [b] Irreversible wave, E_p. [c] CH$_2$Cl$_2$/0.1 M [(*n*-Bu)$_4$N]PF$_6$ solution. [d] sh = shoulder.

reversible oxidations of **10** (Table 3). The oxidation waves of **7** are likely pentathiophene-based processes, since phosphine oxidation is expected at ∼2 V when compared with triphenylphosphine and are in similar positions compared to **10**. Interaction of the oxidized terthienyl group with the phosphino group may contribute to the observed irreversibility. The cyclic voltammogram of **8** (Figure 5c) shows lower ruthenium and thienyl oxidation potentials compared with **1**−**3**. Reduction of **8** shows a wave at −1.22 V that is slightly higher than for **2** and **3** and is most likely a bipyridyl reduction. The second quasi-reversible reduction (−1.36 V) is at a potential higher than would be expected for the second bipyridyl reduction compared to **2** and **3** and may be thienyl-based. The pentathienyl group has a greater ability to accept an electron due to the increased

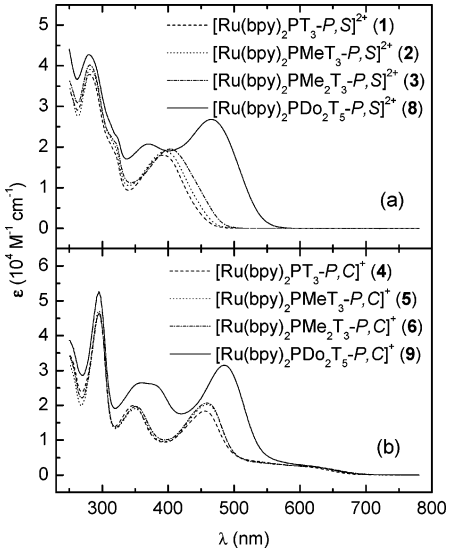

Figure 6. UV−vis spectra of (a) *P*,*S* complexes **1**, **2**, **3**, and **8** and (b) *P*,*C* complexes **4**, **5**, **6**, and **9**. All complexes are PF_6 salts.

conjugation length compared to **2** and **3**. The sharp return peak for **8** indicates a fast process which is characteristic of desorption from the electrode surface. Switching from *P*,*S* to *P*,*C* bonding (**9**) decreases the ruthenium oxidation potential from 1.21 to 0.49 V and significantly lowers the pentathienyl oxidation potentials to 0.80 and 1.46 V. The first thienyl oxidation is at a potential similar to that for **10** (0.82 V), while the second thienyl oxidation is at a potential higher than that for **7** or **10**, but corresponds with the removal of a third electron from the complex. The new wave observed with repeat scans of **9** (0.94 V), similar to that for **4** and **5**, is likely oxidative coupling of the pentathienyl group. Quasireversible (−1.52 V) and irreversible (−1.83 V) reductions are observed that are similar in potential to the bipyridyl reductions observed for **4**−**6**.

UV−Visible Spectroscopy. The UV−vis spectra of the *P*,*S* bound complexes **1**−**3** and **8** are shown in Figure 6a. Bipyridyl $\pi \rightarrow \pi^*$ transitions occur between 280 and 282 nm (Table 4). Terthienyl $\pi \rightarrow \pi^*$ transitions are observed as shoulders at ∼320 nm for **1**−**3**. In comparison, the pentathienyl transition is significantly shifted to 371 nm for **8**, though blue-shifted compared with **7** (406 nm) and **10** (407 nm). Phenyl $\pi \rightarrow \pi^*$ transitions are also expected at around 320 nm and are likely obscured for **1**−**3**. The 323-nm shoulder observed for **8** is in a position similar to the 340-nm phenyl transition observed for PDo_2T_5 (**7**). The Ru d → bpy π^* MLCT transition shifts dramatically with extension of the oligothiophene, from ∼400 nm for **1**−**3** to 465 nm for **8**. These data can be linearly correlated to the electrochemistry data by plotting the MLCT energy converted to electronvolts (E_{op}) versus the difference in potential between the one-electron first oxidation wave of ruthenium and the one-electron reduction potential of the bipyridyl group (ΔE), further substantiating the assignments of the ruthenium oxidation potentials, the bipyridyl first reduction potentials, and the MLCT transitions (Figure S1a).

Solid-state UV−vis spectra of **1**−**3** and **8** were also obtained (Figure S2). MLCT transitions red-shift 19−26 nm for **1**−**3** and 12 nm for **8** compared with solution spectra. Thienyl $\pi \rightarrow \pi^*$ transitions red-shift 6−10 nm, while the bipyridine $\pi \rightarrow \pi^*$ transition remains in the same position for **8**, but red-shifts ∼20 nm for **1**−**3**. Red-shifts in the UV−vis spectra may be due to increased π-orbital overlap related to stacking interactions observed in the crystal structures. Overall, smaller red-shifts are observed for **8**; the presence of the long dodecyl groups may result in a disordered solid state upon drop casting.

Conversion from the *P*,*S* complexes to *P*,*C* complexes **4**−**6** and **9** alters the UV−vis spectra with an accompanying color change from bright yellow or orange to deep brown or red (Figure 6b). For **4**−**6**, there is an approximately 30-nm red-shift for the terthienyl $\pi \rightarrow \pi^*$ transitions compared to **1**−**3**. Additionally, the MLCT transitions red-shift 56−63 nm, and weak "spin-forbidden" MLCT transitions[54−58] are observed as shoulders at 617−633 nm. Switching from *P*,*S* to *P*,*C* bonding does not affect the transitions as strongly in the UV−vis spectra of the pentathienyl complexes as for the terthienyl complexes. The primary MLCT peak red-shifts only 20 nm from **8** to **9**, and the pentathienyl $\pi \rightarrow \pi^*$ transition shifts from 371 nm for **8** to a broad peak at 360 nm with a shoulder at 380 nm for **9**. This fine structure could correspond to conformations of the pentathienyl group that are unable to interconvert rapidly in solution due to the constrained nature of the bonding to ruthenium. This is supported by the observation that the polarity of the solvent affects the relative intensities of these peaks; the peak at 360 nm is more intense in CH_2Cl_2, while the peak at 380 nm is prominent in CH_3CN. Calculations have been reported that predict the ground state of the pentathienyl group is twisted while the excited state is planar (quinoidal); therefore, multiple ground state conformations would result in different $\pi \rightarrow \pi^*$ transition energies.[51] There is also a weak spin-forbidden MLCT transition observed as a shoulder at 615 nm, as was observed for **4**−**6**. The bpy $\pi \rightarrow \pi^*$ transitions of **4**−**6** and **9** at 295 nm are red-shifted from the corresponding *P*,*S* complexes.

There is a linear correlation between the MLCT energies and the ruthenium oxidation and bipyridyl reduction potentials obtained from cyclic voltammetry for **4**−**6** (Figure S1b). Complex **9** displays a large red-shift in the MLCT compared with **4**−**6** but does not show a significant decrease in the oxidation potential of the ruthenium center. This results in a nonlinear correlation between E_{op} and ΔE for **9** compared to **4**−**6**. Correlations of this type are generally valid when charge transfer occurs by a very similar process for complexes in a series, which is evidently not the case for **9**, and could differ due to lower vibrational (χ_i) or solvation (χ_o) reorganizational energies.[59]

Compared to the solution spectra, the solid-state UV−vis spectra of *P*,*C* complexes **4**−**6** and **9** display red-shifts for the bipyridyl (9−20 nm), MLCT (13−26 nm), and thienyl (13−28 nm) transitions that could be due to intramolecular stacking interactions observed in the crystal structures of **4** and **6** (Figure S2). Broader bands are observed that may be due to different equilibrium geometries of the excited states compared to the ground states.[59]

Luminescence Spectroscopy. Excitation of the thienyl $\pi \rightarrow \pi^*$ transition of PDo_2T_5 (**7**) and Do_2T_5 (**10**) produces emission (Table 4) that is slightly red-shifted from that reported for T_5

(54) Lytle, F. E.; Hercules, D. M. *J. Am. Chem. Soc.* **1969**, *91*, 253−257.
(55) Felix, F.; Ferguson, J.; Guedel, H. U.; Ludi, A. *Chem. Phys. Lett.* **1979**, *62*, 153−157.
(56) Felix, F.; Ferguson, J.; Guedel, H. U.; Ludi, A. *J. Am. Chem. Soc.* **1980**, *102*, 4096−102.
(57) Caspar, J. V.; Meyer, T. J. *Inorg. Chem.* **1983**, *22*, 2444−2453.
(58) Mamo, A.; Stefio, I.; Poggi, A.; Tringali, C.; Di Pietro, C.; Campagna, S. *New J. Chem.* **1997**, *21*, 1173−1185.
(59) Dodsworth, E. S.; Lever, A. B. P. *Chem. Phys. Lett.* **1986**, *124*, 152−158.

Table 4. UV−Vis and Luminescence Data

compound	UV–vis[a] λ_{max}, nm [($\epsilon \pm 0.01 \times 10^4$) M^{-1} cm^{-1}]	luminescence[b] λ_{max}, nm
$[Ru(bpy)_2PT_3\text{-}P,S]^{2+}$ (**1**)	280 (3.79×10^4), 320 (sh)[e] (1.83×10^4), 393 (1.80×10^4)	−
$[Ru(bpy)_2PMeT_3\text{-}P,S]^{2+}$ (**2**)	282 (3.91×10^4), 320 (sh)[e] (1.97×10^4), 396 (1.89×10^4)	−
$[Ru(bpy)_2PMe_2T_3\text{-}P,S]^{2+}$ (**3**)	282 (4.01×10^4), 320 (sh)[e] (2.11×10^4), 404 (1.95×10^4)	−
$[Ru(bpy)_2PT_3\text{-}P,C]^{+}$ (**4**)	295 (4.63×10^4), 347 (2.00×10^4), 456 (1.84×10^4), 617 (sh)[e] (2.25×10^3)	754 ($\tau = 22 \pm 2$ ns)[c]
$[Ru(bpy)_2PMeT_3\text{-}P,C]^{+}$ (**5**)	295 (4.72×10^4), 350 (1.91×10^4), 459 (2.03×10^4), 628 (sh)[e] (2.20×10^3)	763
$[Ru(bpy)_2PMe_2T3\text{-}P,C]^{+}$ (**6**)	295 (4.64×10^4), 351 (1.97×10^4), 460 (2.07×10^4), 633 (sh)[e] (2.10×10^3)	772
PDo_2T_5 (**7**)	251 (2.13×10^4), 340 (sh)[e] (1.47×10^4), 406 (3.36×10^4)	499, 528
$[Ru(bpy)_2PDo_2T_5\text{-}P,S]^{2+}$ (**8**)	280 (4.27×10^4), 323 (sh)[e] (2.24×10^4), 371 (2.07×10^4), 465 (2.68×10^4)	602 ($\tau < 10$ ns)[d]
$[Ru(bpy)_2PDo_2T_5\text{-}P,C]^{+}$ (**9**)	295 (5.24×10^4), 360 (2.63×10^4), 380 (sh)[e] (2.59×10^4), 485 (3.15×10^4), 615 (sh)[e] (2.62×10^3)	−
Do_2T_5 (**10**)	252 (1.27×10^4), 407 (3.27×10^4)	487, 516

[a] Measurements carried out in CH_2Cl_2 solution. [b] Degassed CH_3CN solution. [c] Lifetime determined from emission at 750 nm. [d] Lifetime determined from emission at 600 nm. [e] sh = shoulder.

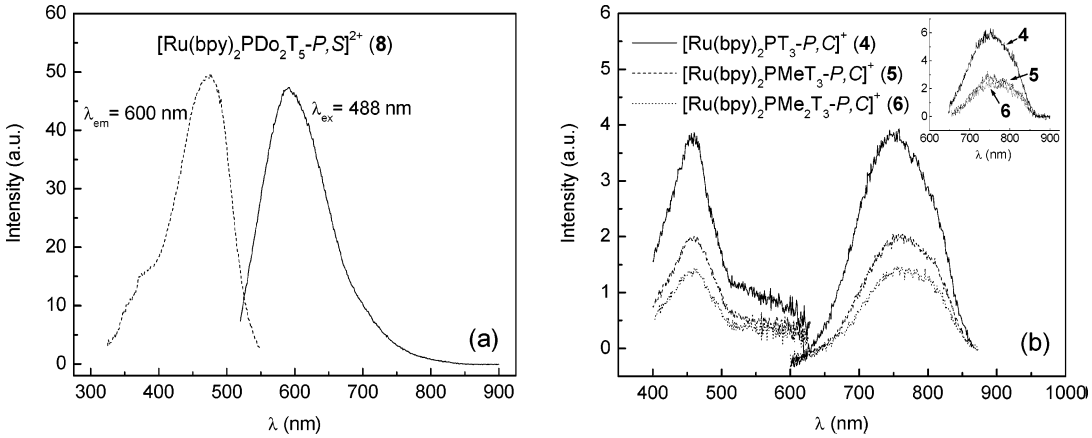

Figure 7. Emission and excitation spectra of (a) **8** and (b) *P*,*C* complexes **4** ($\lambda_{ex} = 456$ nm, $\lambda_{em} = 748$ nm), **5** ($\lambda_{ex} = 459$ nm, $\lambda_{em} = 751$ nm), and **6** ($\lambda_{ex} = 460$ nm, $\lambda_{em} = 761$ nm) in deaerated CH_3CN. The inset shows emission where $\lambda_{ex} = 616$ nm for **4** and **5**, and $\lambda_{ex} = 620$ nm for **6**. All solutions abs = 0.1 at the excitation wavelength and the solvent spectra have been subtracted for clarity.

(482, 514 nm, $\phi = 0.54$).[60] The approximate quantum yields of the emission from **7** and **10** are 0.093 and 0.16, respectively, measured by comparison to T_3 in CH_3CN ($\phi = 0.056$).[51] Complexation of the oligothienyl groups to $Ru(bpy)_2$ quenches the thienyl-based fluorescence. Luminescence, which is generally observed from the MLCT excited state for complexes containing the $Ru(bpy)_2$ fragment, is quenched for **1**−**3**, possibly due to thermal population of a low-lying nonemissive energy level (vide infra). The very weak luminescence from the MLCT state of **8** at 602 nm (approximate quantum yield of 0.01%) is shown in Figure 7a. The luminescence lifetime of **8** was measured at 600 nm; however, the lifetime was shorter than the lower limit measurable with the instrumentation used. Thus, the lifetime of **8** is less than 10 ns. The short emission lifetime compared with $[Ru(bpy)_3]^{2+}$ ($\tau = 870$ ns) and other $[Ru(bpy)_2(LL)]^{2+}$ complexes[39] and the low quantum yield support the conclusion that either significant thermal population of a low-lying, nonemissive d−d state is occurring or vibrational relaxation pathways are competitive with emission from the MLCT state. When the bonding mode is switched from *P*,*S* to *P*,*C*, there are changes in the luminescence that are related to shifting of the MLCT levels. Complexes **4**−**6** have a low-lying MLCT level available and display low-energy emission at 754−772 nm. Approximate quantum yields are ∼0.001% and decrease in intensity with the addition of methyl substituents (Figure 7b). The emission lifetime of **4** was measured at 750 nm and was determined to be 22 ± 2 ns (Figure S4a). A short-lived (<10 ns, Figure S4a) species was observed for **4** that emits below 620 nm (Figure S4b). This emission decays within the laser pulse and is much shorter lived than the emission at 750 nm; it is likely due to the formation of a decomposition product (vide infra). $[Ru(bpy)_2PDo_2T_5\text{-}P,C]PF_6$ (**9**) does not display any observable emission, which, combined with the decrease in intensity with the addition of methyl substituents, indicates that there is increased deactivation of the excited state with an increase in vibrational modes.

Earlier, emission at ∼450 nm for **1**, **3**, **4**, and **6** was reported.[26] We have now determined that higher energy emission is

(60) Fichou, D. *Handbook of Oligo- and Polythiophenes*; Wiley-VCH: Weinheim, Germany, 1999.

observed as a result of small amounts of side product that form in solution and exhibit more intense ligand-like emission. These side products form more rapidly in chlorinated solvents such as $CHCl_3$ or CH_2Cl_2 than in CH_3CN or acetone. Since the MLCT states are expected to be the lowest energy states,[21] the appearance of higher-energy emission suggests that the ligand detaches from the metal. Complex **8** displays a new luminescence band at 514 nm shortly after dissolution in CH_3CN (Figure S5), and the excitation and emission spectra and higher intensity of this new luminescence match those of PDo_2T_5 (**7**). The side products appear to form in very small concentrations and are not easily observed by techniques other than emission measurements or at higher concentrations in solution. The side product is not observed for **8** at higher concentrations (~25 mM) by ^{31}P NMR spectroscopy; after 11 days in $CO(CD_3)_2$, there are no new peaks in the spectrum. Complex **9** shows greater instability in solution compared to **8**, and the ^{31}P NMR in $CO(CD_3)_2$ shows a minor peak at δ 41.2 after 1 h in $CO(CD_3)_2$ and multiple minor peaks are formed after 24 h. Similar results were observed for the terthienyl complexes, though side products form less rapidly. ^{31}P NMR experiments show that the side products formed by the *P*,*S* or *P*,*C* complexes in solution disappear with the addition of concentrated acid, to reform only the *P*,*S* complex. These experiments suggest that there is an equilibrium between the complexes and the side products.

Discussion

The elongated lengths (0.011−0.043 Å) of the S−C bonds of the bound thienyl ring in the solid-state structures of *P*,*S* complexes **1**, **3**, and **8** relative to calculated bond lengths of terthiophene[42] indicate that the sulfur atom is partially or fully removed from conjugation, as expected due to sp^3 hybridization of a thienyl sulfur bound to a metal. Bond length changes of the C−C bonds in the bound ring are <0.01 Å; therefore, complexation of the thienyl sulfur would not be expected to interrupt conjugation across all of the rings. Despite the large tilt angles (53.7−58.4°) observed for the *P*,*S* complexes and the preferred orientation of the bound thienyl rings coinciding with intramolecular π-stacking between the phenyl and thienyl rings, both torsion angles between the adjacent rings of **1** are close in value to that of terthiophene (147.6°).[42] Complex **3** has a more coplanar conformation, which would be expected as a result of electron donation by the methyl substituents. The torsion angle between the bound rings of **8** is equivalent to that of terthiophene, while the exterior rings align cis and trans and with multiple conformations, similar to T_5.[51] These results suggest that the alterations of properties of the oligothienyl groups upon *P*,*S* complexation with $Ru(bpy)_2$ are mainly electronic in nature rather than steric.

A decrease in electron density across the rings is indicated by a ~35 nm blue-shift of the thienyl $\pi \rightarrow \pi^*$ transitions of **1**−**3** and **8** compared to the terthienyl ligands[28] and **7**, and is likely due to a combination of decreased electron density at the ring coordinated to a Ru^{II} center and possibly near the complexed phosphino group. Removal of electron density from the thienyl rings is consistent with thienyl oxidation waves (>1.69 V) that are substantially higher in potential compared with the terthienyl ligands (1.05−1.30 V)[28] or **7** (0.99 V), and which would contribute to larger thienyl $\pi \rightarrow \pi^*$ energy gaps, as observed in the UV−vis spectra. Complexation to $Ru(bpy)_2$ also removes sufficient electron density to increase the terthienyl reduction potentials of **2** and **3**, shown by the reversible third reduction waves observed at −1.79 and −1.81 V. The Ru−S bond length of the *P*,*S* complexes can be correlated to the availability of electron density in the oligothienyl rings; **3** and **8** show 0.0019 and 0.0043 Å reductions, respectively, in the Ru−S bond lengths compared to **1**.

When the complexes are switched to the *P*,*C* bonding mode, a forced π-antibonding orbital overlap between ruthenium and the bound thienyl rings is indicated in the solid-state structures of **4** and **6**. The hybridization at the bound carbon does not allow significant deviation from a trigonal arrangement; therefore, there is only a 9−10° tilting of the bound ring and 0.033−0.042 Å elongation of the $C_{35}-C_{36}$ bonds of **4** and **6** compared to **1** and **3**. While there is clearly a disruption of conjugation around the bound thienyl rings, there are marked increases in coplanarity of the three thienyl rings when **1** and **3** are converted to **4** and **6**. The *P*,*C* complexes are also electron-rich as a result of the loss of a proton during the cyclometalation reaction, and the overall charge of the complexes is +1 rather than +2. This is reflected by the 0.7−0.9 V decrease in the thienyl oxidation potentials compared to the *P*,*S* complexes to yield oxidations at 1.11, 1.04, 0.96, and 0.80 V for **4**−**6** and **9**, respectively. Overall, the thienyl ligands of **4**−**6** are more electron-rich and more coplanar than those in **1**−**3**, resulting in ~30-nm red-shifts of the thienyl $\pi \rightarrow \pi^*$ transitions.

The two thienyl $\pi \rightarrow \pi^*$ transitions at 360 and 380 nm that are observed for **9** are not significantly removed from the transition for **8** (371 nm), and both transitions are still blue-shifted from **7** (406 nm). Pentathiophenes do not normally show conformational structure in solution, but it is observed at low temperature,[51] and the *P*,*C* bonding mode may result in a barrier to interconversion between two conformers. The presence of a conformer of **9** that is blue-shifted from **8** indicates poor π-overlap of the orbitals and a less planar structure, though the orientation of the rings is unknown since a solid-state structure for **9** could not be obtained. Interconversion between two conformers that could be present would still be relatively fast since only single peaks are observed by ^{31}P NMR spectroscopy and cyclic voltammetry at room temperature. It has been established that for both bonding modes, complexation of the metal affects the conjugation of the thienyl rings and related properties but does not remove the ring from π-conjugation with the unbound rings, as has been observed for other metal-bound thienyl systems.[61]

It is evident that the C−H bond cleavage that occurs during the cyclometalation reaction involves the ruthenium center. Formally, the cyclometalation reaction is a deprotonation, and reversion to a *P*,*S* complex is protonation; however, oligothiophenes are not normally deprotonated by NaOH. Mo/Co catalysts are known to promote dehydrosulfurization of thienyl rings, and activation of C−H bonds on thienyl rings has been reported for Ru, Re, and Rh complexes.[33,34,62,63] In these studies, migration of a metal from sulfur to carbon on the ring is observed, and the suggested mechanism of C−H activation via the formation of a η^2-coordinated intermediate is supported. In the presence of base, the metal may migrate to the inner C−C

(61) Graf, D. D.; Mann, K. R. *Inorg. Chem.* **1997**, *36*, 150−157.
(62) Dong, L.; Duckett, S. B.; Ohman, K. F.; Jones, W. D. *J. Am. Chem. Soc.* **1992**, *114*, 151−160.
(63) Angelici, R. J. *Organometallics* **2001**, *20*, 1259−1275.

double bond in the *P*,*S* complexes, and the removal of electron density from the ring is expected to promote deprotonation, providing a site on the thienyl ring for carbon−metal bonding.

The thienyl groups bound in different modes also affect the properties of the attached $Ru(bpy)_2$ group. Compared to the oxidation potential of $[Ru(bpy)_3]^{2+}$ (1.01 V versus SCE),[39] oxidation potentials are >0.40 V higher for the *P*,*S* complexes, which suggests poor electron donation from a thienyl sulfur and phosphine compared to a pyridine ring. The MLCT absorptions are also blue-shifted 50 nm compared to $[Ru(bpy)_3]^{2+}$ (452 nm),[39] which is consistent with phosphine coordination destabilizing the MLCT state to a greater extent than for pyridine coordination, as has been reported,[57] while the effect of coordination of the thienyl sulfur on the MLCT state is unknown. The 0.72−0.92 V decrease in the ruthenium oxidation potentials when the bonding is switched from *P*,*S* to *P*,*C* reflects the substantial increase in electron donation from the thienyl carbon. Lower oxidation potentials have been observed for other cyclometalated Ru complexes.[38,64] The effect of switching on the bipyridyl reduction potentials is only a 0.20−0.32 V decrease and a 13-nm red-shift of the $\pi \rightarrow \pi^*$ transition. Since the bonding mode more strongly affects the ruthenium oxidation potential, there is a contraction of the energy differences between the ruthenium oxidation and the first bipyridyl reduction, which are known to correlate to the MLCT transitions of $[Ru(bpy)_3]^{2+}$ complexes.[59,65] The lowering of the Ru^{II} oxidation potentials results in 56−63-nm red-shifts in the MLCT for **4**−**6**, and a 20-nm red-shift for **9**. The low energy band that is observed for the *P*,*C* complexes is a transition to a low-lying state that is mostly triplet in character. Transition to a low-lying "forbidden" level is observed as a relatively strong transition in osmium polypyridine complexes[57,58,66] due to spin−orbit coupling,[54,67,68] and as a much weaker transition in $[Ru(bpy)_3]^{2+}$ [54−56] and some $[Ru(bpy)_2(LL)]^{2+}$ complexes.[57,58] This transition, due to its very weak intensity, is often covered by superimposed, allowed MLCT transitions that are much stronger in intensity. The weak, low-lying state is likely underneath the symmetry-allowed MLCT transitions for the *P*,*S* complexes; therefore, at wavelengths <550 nm. In the *P*,*C* bonding mode, this transition is dramatically shifted to longer wavelengths to form a broad shoulder observed for all *P*,*C* complexes, extending to 700 nm and covering the visible range, similar to $Ru(bpy)_2L_2$ complexes that have been synthesized as black absorbers for possible applications in photovoltaic cells.[69,70] The anionic character of the cyclometalated oligothienyl ligands stabilizes the excited states by electron donation to Ru^{III} to shift the bands, which has also been observed in Ru/Os polypyridine complexes.[58,66] The overall effect of stabilizing the Ru^{III} excited state, a reduction in the MLCT absorption energy, is the same as incorporating a bpy-type acceptor ligand.[71]

It is generally accepted that, in $Ru(bpy)_2L_2$, $Os(bpy)_2L_2$ and related complexes, absorption is primarily to a singlet-based MLCT state and emission is from a triplet-based MLCT state, with spin−orbit coupling mixing the singlet and triplet states.[21,57,66,72] It was found that *P*,*S* complexes **1**−**3** do not emit; therefore, the MLCT-based luminescence is quenched. This quenching of the MLCT emission is observed in systems containing phosphines due to destabilization of the MLCT state without destabilization of a low-lying, metal-centered dd state.[57,65] This results in a low barrier for energy transfer to the nonemissive dd state and a major deactivation route at room temperature. Weak emission is observed at 602 nm for the *P*,*S* pentathienyl complex **8** that is expected to have a stabilized MLCT* state according to the red-shifted transition energy; therefore, there may be a higher barrier to the dd state compared with **1**−**3**. A low-lying, ligand-based triplet state has been observed in other thienyl/$Ru(bpy)_2$ systems,[21] resulting in a weakly emitting MLCT state with a characteristically longer lifetime; however, the observation of a substantially shorter lifetime (<10 ns) for **8** than is normally observed for $Ru(bpy)_2$ complexes is in accordance with the presence of an accessible nonemissive dd state. For the *P*,*C* complexes, very weak luminescence that approaches the near-infrared region (754−772 nm) is observed for **4**−**6** but not for **9**. The emission is from a "forbidden" MLCT state that should be low enough in energy to create a barrier to a low-lying dd level. Lowering of the MLCT state when switching to the *P*,*C* bonding mode is due to the formation of a more electron-rich complex, which has been observed to promote luminescence in another $Ru(bpy)_2L_2$ switchable system.[73] The reduction in intensity of emission from **4** to **6** and the absence of emission for **9** are likely due to competing nonradiative relaxation that increases with increasing vibrational modes introduced by the addition of alkyl substituents to the ligands and is in accordance with the energy gap law.[74,75] The short 22 ± 2 ns lifetime observed for the emission of **4** is also in agreement with the presence of competing deactivation pathways. The complexes display *P*,*S* −ON, *P*,*C* −OFF emission behavior for the pentathienyl complexes **8** and **9**, respectively, and *P*,*S* −OFF, *P*,*C*- ON emission behavior for the terthienyl complexes **1**−**3** and **4**−**6**, respectively.

Crystalline and drop-cast solid-state samples of *P*,*S* and *P*,*C* complexes display stability in air and under UV and visible light. There may be contributions from the intra- and intermolecular π-stacking of the bpy, phenyl, and thienyl rings toward the stability of the complexes. Bound $Ru(bpy)_2$ groups could be used to dope the thienyl chains via the Ru → bpy MLCT, provided there was effective overlap of the ruthenium and thienyl oxidation potentials, and we are currently investigating this approach. Additionally, π-stacking of the terthienyl complexes between thienyl rings potentially would increase conductivity of an oxidatively doped oligomeric solid. Complexes containing longer oligothiophene chains or polythiophene would improve the processibility and flexibility of these materials, and disordered systems would also create materials with new properties.

(64) Beley, M.; Collin, J. P.; Louis, R.; Metz, B.; Sauvage, J. P. *J. Am. Chem. Soc.* **1991**, *113*, 8521−8522.
(65) Sullivan, B. P.; Salmon, D. J.; Meyer, T. J. *Inorg. Chem.* **1978**, *17*, 3334−3341.
(66) Mamo, A.; Juris, A.; Calogero, G.; Campagna, S. *Chem. Commun.* **1996**, 1225−1226.
(67) Kober, E. M.; Meyer, T. J. *Inorg. Chem.* **1984**, *23*, 3877−3886.
(68) Kober, E. M.; Meyer, T. J. *Inorg. Chem.* **1983**, *22*, 1614−1616.
(69) Anderson, P. A.; Strouse, G. F.; Treadway, J. A.; Keene, F. R.; Meyer, T. J. *Inorg. Chem.* **1994**, *33*, 3863−3864.
(70) Anderson, P. A.; Keene, F. R.; Meyer, T. J.; Moss, J. A.; Strouse, G. F.; Treadway, J. A. *J. Chem. Soc., Dalton Trans.* **2002**, 3820−3831.
(71) Rillema, D. P.; Mack, K. B. *Inorg. Chem.* **1982**, *21*, 3849−3854.
(72) Kober, E. M.; Sullivan, B. P.; Meyer, T. J. *Inorg. Chem.* **1984**, *23*, 2098−2104.
(73) Wang, K.-Z.; Gao, L.-H.; Bai, G.-Y.; Jin, L.-P. *Inorg. Chem. Commun.* **2002**, *5*, 841−843.
(74) Caspar, J. V.; Meyer, T. J. *J. Am. Chem. Soc.* **1983**, *105*, 5583−5590.
(75) Caspar, J. V.; Meyer, T. J. *J. Phys. Chem.* **1983**, *87*, 952−957.

Conclusions

The effect of the two bonding modes, *P*,*S* and *P*,*C*, on the electrochemical and spectroscopic properties of oligothiophenes has been examined. The *P*,*S* coordinated complexes exhibit properties different from those of the thienyl ligands, indicated by a blue-shift in the thienyl absorption bands, as well as large increases in oxidation potentials. Switching to the *P*,*C* bonding mode lowers the thienyl oxidation potentials to less than those in the corresponding ligands. Because of a combination of a more electron-rich system and increased planarity of the thienyl chains with *P*,*C* bonding, there are large red-shifts observed for the terthienyl $\pi \rightarrow \pi^*$ transitions compared to the *P*,*S* complexes. There is a smaller red-shift for the pentathienyl $\pi \rightarrow \pi^*$ transition with switching from *P*,*S* to *P*,*C* bonding that indicates a difference in the conformation of the *P*,*C* bound pentathienyl group compared to the *P*,*C* bound terthienyl groups, which could be due to steric interaction between the two external rings or the dodecyl substituents. All of the *P*,*C* bound complexes can be reverted to the *P*,*S* bound form by the addition of acid; therefore, the two bonding modes are reversibly switchable. The Ru → bpy MLCT emission observed from these complexes is too weak for most applications; however, the results demonstrate how switching the binding mode affects the observation of luminescence from the MLCT level, and for the *P*,*C* bound complexes, the luminescence emission wavelengths can be pushed to the near-IR region. Compared to the oligothienyl ligands, the electrochemical and photophysical properties of the *P*,*S* complexes are primarily influenced by electronic interactions, while the properties observed for the *P*,*C* complexes are due to both electronic interactions and steric effects. In metal−thienyl systems, oxidation or ligand exchange at the metal is used to affect the properties of the complexed oligo- or polythiophene; however, we have found that switching of the binding mode provides an effective handle to substantially alter the electrochemical and the photophysical properties of the thienyl chain. Solid-state films of these complexes would have potential as conductors, with the advantageous ability to affect the properties of the thienyl groups through interaction with the metal. Results encourage further investigation of the effect of direct coordination of metals to an oligothiophene or polythiophene backbone on the electronic properties.

Experimental Section

General. All reactions were performed using standard Schlenk techniques with dry solvents under nitrogen. PT_3, $PMeT_3$, and PMe_2T_3 were prepared according to published procedures,[28] as were [Ru(bpy)$_2$PT$_3$-*P*,*S*](PF$_6$)$_2$ (**1**) and [Ru(bpy)$_2$PMe$_2$T$_3$-*P*,*S*](PF$_6$)$_2$ (**3**).[26] Previously reported complexes [Ru(bpy)$_2$PT$_3$-*P*,*C*]PF$_6$ (**4**) and [Ru(bpy)$_2$PMe$_2$T$_3$-*P*,*C*]PF$_6$ (**6**)[26] have been prepared by the revised procedure used to prepare [Ru(bpy)$_2$PMeT$_3$-*P*,*C*]PF$_6$ (**5**) with improved yields (50−85%). All other reagents were purchased from Aldrich or Strem Chemicals. *N*,*N*′-Dimethylethylenediamine, bis-2-methoxyethyl ether, and xylenes were distilled before use. All other reagents were used as received. ^{1}H and ^{31}P NMR experiments were performed on either a Bruker AV-300 or a Bruker AV-400 Spectrometer, and spectra were referenced to residual solvent (^{1}H) or external 85% H_3PO_4 (^{31}P). UV−visible spectra were obtained on a Cary 5000 in HPLC grade CH_2Cl_2. Emission spectra were obtained on a Cary Eclipse in HPLC grade CH_2Cl_2 or CH_3CN, and emission slits were opened to 20 nm for measurement of metal complexes. Cyclic voltammetry experiments were carried out on a Pine AFCBP1 bipotentiostat using a Pt disk working electrode, Pt coil wire counter electrode, and a silver wire reference electrode. Either decamethylferrocene or ferrocene was used as an internal reference to correct the measured potentials with respect to saturated calomel electrode (SCE). The supporting electrolyte was 0.1 M [(*n*-Bu)$_4$N]PF$_6$ that was purified by recrystallizing three times from ethanol and drying for 3 days at 90 °C under vacuum. Lifetime measurements were obtained by exciting samples at 480 nm in 7 × 7 mm Suprasil cells at 20 ± 2 °C with a Coherent Infinity OPO tunable laser, using the laser flash photolysis system previously described.[76] Deoxygenated samples were dissolved in acetonitrile to achieve absorbances between 0.3 and 0.5 (l = 7 mm) at 480 nm. Emission decays were measured at fixed wavelengths, averaging at least 5 kinetic traces, and emission spectra were obtained by collecting data at fixed wavelengths and averaging the values between set time windows after the laser pulse. The voltage on the photomultiplier used to detect the emission signal was kept constant throughout the collection of a spectrum.

[Ru(bpy)$_2$PMeT$_3$-*P*,*S*](PF$_6$)$_2$ (2). $AgBF_4$ (230 mg, 1.15 mmol) was added to a deaerated solution of Ru(bpy)$_2$Cl$_2$·2H$_2$O (300 mg, 0.576 mmol) in acetone (30 mL), stirred for 6 h, and filtered under nitrogen. To the red filtrate 3′-(diphenylphosphino)-5-methyl-2,2′:5′,2″-terthiophene ($PMeT_3$) (272 mg, 0.610 mmol) was added, and the mixture was heated to reflux for 18 h. The resulting solution was concentrated to 10 mL and precipitated by addition to a solution of NH_4PF_6 (1.89 g, 11.6 mmol) in 100 mL of H_2O. Recrystallization in 9:1 ethanol−acetone gave **2** as bright, pale orange crystals. Yield: 0.340 g (51%). ^{1}H NMR (300.1 MHz, CO(CD$_3$)$_2$): δ 9.13 (d, J = 5.7 Hz, 1H), 8.89 (d, J = 5.2 Hz, 1H), 8.78 (d, J = 8.2 Hz, 1H), 8.69 (d, J = 7.5 Hz, 1H), 8.68 (d, J = 8.1 Hz, 1H), 8.60 (d, J = 8.2 Hz, 1H), 8.28−8.22 (m, 3H), 8.09 (t, J = 8.0 Hz, 1H), 7.96 (d, J = 5.7 Hz, 1H), 7.83−7.81 (m, 1H), 7.69 (t, J = 6.9 Hz, 1H), 7.63−7.55 (m, 3H), 7.50 (d, J = 5.0 Hz, 2H), 7.45−7.32 (m, 6H), 7.22−7.16 (m, 3H), 708 (dd, J = 4.8 Hz, J = 3.9 Hz, 1H), 6.95−6.88 (m, 3H), 6.78−6.77 (m, 1H), 1.48 (s, 3H). ^{31}P{^{1}H} NMR (121.5 MHz, CO(CD$_3$)$_2$): δ 28.5 (s), −143.0 (septet, J_{PF} = 708 Hz, PF_6). Anal. $C_{45}H_{35}F_{12}N_4S_3P_3Ru$ requires C, 47.00; H, 3.07. Found: C, 46.60; H, 3.05%.

[Ru(bpy)$_2$PMeT$_3$-*P*,*C*]PF$_6$ (5). NaOH (0.72 g, 18 mmol) was dissolved in deaerated methanol (18 mL) to give a 1.0 M solution. **2** (0.600 g, 0.521 mmol) was dissolved into the solution and stirred at reflux for 18 h. A color change from yellow to dark brown was observed. The solution was then cooled to room temperature, concentrated to 10 mL, and pipetted dropwise into a solution of NH_4PF_6 (1.70 g, 10.4 mmol) in H_2O (90 mL) to form a brownish-black precipitate. The precipitate was isolated by filtration, washed with water (10 mL) and then ether (15 mL), and recrystallized in 9:1 ethanol−acetone to give **5** as black, shiny crystals. Yield: 0.376 g (72%). ^{1}H NMR (400.1 MHz, CO(CD$_3$)$_2$): δ 8.85 (m, 1H), 8.56−8.49 (m, 2H), 8.42−8.38 (m, 3H), 8.03 (m, 1H), 7.92 (m, 2H), 7.83 (m, 2H), 7.6−7.61 (m, 3H), 7.41 (m, 5H), 7.32 (m, 1H), 7.24 (m, 1H), 7.12 (m, 2H), 7.02 (m, 1H), 6.89 (m, 3H), 6.61 (m, 1H), 6.49 (m, 2H), 6.06 (m, 1H) 2.16 (s, 3H). ^{31}P{^{1}H} NMR (162.0 MHz, CO(CD$_3$)$_2$): δ 44.9 (s), −143.0 (septet, J_{PF} = 708 Hz, PF_6). Anal. $C_{49}H_{34}F_6N_4S_3P_2Ru$ requires C, 53.83; H, 3.41. Found: C, 54.04; H, 3.49%.

3″-Bromo-3,3‴′-didodecyl-2,2′:5′,2″:5″,2‴:5‴,2‴′-pentathiophene (BrDo$_2$T$_5$). Mg (1.36 g, 56 mmol) and I_2 (5 mg, 0.02 mmol) were brought to reflux in 60 mL of THF, and 2-bromo-3-dodecylthiophene (9.29 g, 28 mmol) dissolved in THF (10 mL) was slowly added by syringe. The green-brown mixture was heated at reflux for 2 h and allowed to cool. The Grignard solution was then slowly added by cannula to a condenser-fitted flask containing 5,3′,5″-tribromo-2,2′:5′,2″-terthiophene (6.79 g, 14 mmol), Pd(dppf)Cl$_2$·CH$_2$Cl$_2$ (300 mg, 0.367 mmol), diethyl ether (80 mL), and toluene (60 mL). The yellow-brown solution was heated at reflux for 16 h and then quenched with saturated aq. NH_4Cl and stirred for 1 h. The crude product was extracted with CH_2Cl_2 and washed with saturated $NaHCO_3$ once and

(76) Liao, Y.; Bohne, C. *J. Phys. Chem.* **1996**, *100*, 734−743.

then three times with water to give a bright orange solution that was condensed to give an orange-red oil. The crude product was run through a short silica gel plug with hexanes to remove side product (3-dodecylthiophene) and catalyst, and then it was purified by column chromatography on silica gel with hexanes. The initial yellow band was a mixture of tetrathiophene side products. The second orange band was collected, and the solvent was removed to give $BrDo_2T_5$ as a soft, waxy bright orange solid. Yield: 7.61 g (66%). ^{1}H NMR (200.1 MHz, $CDCl_3$): δ 7.37 (d, J = 5.4 Hz, 1H), 7.18 (d, J = 7.7 Hz, 2H), 7.11 (d, J = 5.7 Hz, 1H), 7.07 (s, 1H), 7.06 (d, J = 5.7 Hz, 1H), 7.01 (d, J = 5.4 Hz, 1H), 6.93 (d, J = 7.8 Hz, 2H), 2.77 (m, 4H), 1.65 (m, 4H), 1.25 (m, 36H), 0.87 (t, J = 6.8 Hz, 6H). Anal. $C_{44}H_{59}S_5Br$ requires C, 72.09; H, 8.67. Found: C, 72.10; H, 8.97%.

3,3‴′-Didodecyl-3″-iodo-2,2′:5′,2″:5″,2‴:5‴,2⁗-pentathiophene (IDo_2T_5). NaI (2.75 g, 18.36 mmol), CuI (87.5 mg, 0.459 mmol), and $BrDo_2T_5$ (7.61 g, 9.18 mmol) were dissolved in xylenes/bis-2-methoxyethyl ether (160 mL/40 mL). The addition of *N*,*N*′-dimethylethylenediamine (0.098 mL, 81 mg, 0.92 mmol) caused a white precipitate to form, and the resulting mixture was heated to 165 °C for 16 h. After cooling, a dark yellow organic layer and a green aqueous layer were formed with the addition of CH_2Cl_2 and water. The organic layer was separated, washed three times with water, dried with $MgSO_4$, and filtered. The solvent was removed, and the xylenes and bis-2-methoxyethyl ether were distilled away to leave an oily crude product. Purification by column chromatography on silica gel with hexanes gave IDo_2T_5 as a soft, waxy bright orange solid after removal of solvent. Yield: 7.58 g (94%). ^{1}H NMR (200.1 MHz, $CDCl_3$): δ 7.38 (d, J = 4.0 Hz, 1H), 7.19−7.16 (m, 2H), 7.16 (s, 1H), 7.11 (d, J = 3.6 Hz, 1H), 7.08 (d, J = 4.0 Hz, 1H), 7.01 (d, J = 3.8 Hz, 1H), 6.93 (d, J = 5.2 Hz, 2H), 2.77 (m, 4H), 1.65 (m, 4H), 1.25 (m, 36H), 0.87 (t, J = 6.6 Hz, 6H). Anal. $C_{44}H_{59}S_5I$ requires C, 60.38; H, 6.79. Found: C, 60.78; H, 6.88%.

3,3‴′-Didodecyl-3″-diphenylphosphino-2,2′:5′,2″:5″,2‴:5‴,2⁗-pentathiophene (PDo_2T_5, 7). [$Pd(OCOCH_3)_2$] (5 mg, 0.022 mmol) and IDo_2T_5 (4.33 g, 4.95 mmol) were dissolved in acetonitrile (250 mL), and distilled triethylamine (1.4 mL, 1.0 g, 9.9 mmol) was injected into the flask. The orange suspension darkened to a greenish-brown with heating at reflux for 16 h, and a black, gelatinous layer was formed on the flask bottom. Solvent and volatiles were removed under reduced pressure, and the crude product was extracted with CH_2Cl_2 and washed with 1 M aq KOH, 2 M aq HCl, then three times with water. Removal of solvent left a brown oil. Purification by column chromatography on silica gel with acetone−hexanes (5/95) resulted in elution of starting material IDo_2T_5, followed by **7** as an orange band, and an orange band containing the phosphine oxide eluting much later. The isolated product was a bright orange oil after removal of solvent. Yield: 4.29 g (93%). ^{1}H NMR (200.1 MHz, $CDCl_3$): δ 7.37 (m, 10H, phenyl), 7.15 (d, J = 5.2 Hz, 2H), 7.03 (d, J = 3.6 Hz, 1H), 7.01 (d, J = 4.0 Hz, 1H), 6.99 (d, J = 4.4 Hz, 1H), 6.96, (d, J = 3.8 Hz, 1H), 6.91 (d, J = 5.0 Hz, 2H), 6.63 (s, 1H), 2.73 (m, 4H), 1.61 (m, 4H), 1.25 (m, 36H), 0.87 (m, 6H). ^{31}P{^{1}H} NMR (81.0 MHz, $CDCl_3$): δ −23.5 (s). Anal. $C_{56}H_{69}S_5P$ requires C, 72.05; H, 7.45. Found: C, 71.65; H, 7.49%.

[$Ru(bpy)_2PDo_2T_5$-*P*,*S*]$(PF_6)_2$ (8). $AgBF_4$ (1.79 g, 9.18 mmol) was added to a deaerated solution of $Ru(bpy)_2Cl_2 \cdot 2H_2O$ (2.39 g, 4.59 mmol) in acetone (150 mL), stirred for 3 h, and filtered under nitrogen. The resulting red filtrate was added to a suspension of **7** (4.29 g, 4.60 mmol) in deaerated acetone (25 mL), and the mixture was heated at reflux for 20 h. The resulting solution was condensed to 30 mL and pipetted dropwise into a solution of NH_4PF_6 (15 g, 92 mmol) in H_2O (300 mL) and stirred for 0.5 h to give dark orange precipitate. The precipitate was recovered and dissolved in acetone, the remaining solids were filtered off, and the solvent was removed. Recrystallization in 9:1 ethanol−acetone gave **8** as bright orange crystals. Yield: 3.44 g (46%). ^{1}H NMR (400.1 MHz, $CO(CD_3)_2$): δ 9.25 (d, J = 6.0 Hz, 1H), 9.09 (d, J = 5.6 Hz, 1H), 8.71 (d, J = 7.6 Hz, 1H), 8.63 (d, J = 7.6 Hz, 1H), 8.58 (d, J = 8.0 Hz, 1H), 8.55 (d, J = 8.4 Hz, 1H), 8.31 (t, J = 8.0 Hz, 1H), 8.25 (t, J = 8.0 Hz, 1H), 8.05 (t, J = 7.8 Hz, 1H), 7.80 (t, J = 8.0 Hz, 1H), 7.81 (d, J = 5.6 Hz, 1H), 7.75 (t, J = 6.6 Hz, 1H), 7.64−7.60 (m, 2H), 7.55−7.48 (m, 2H), 7.46 (d, J = 4.0 Hz, 1H), 7.42−7.38 (m, 5H, phenyl), 7.30 (t, J = 6.8 Hz, 1H), 7.25−7.22 (m, 3H), 7.18 (d, J = 5.2 Hz, 1H), 7.14 (d, J = 4.0 Hz, 1H), 7.08 (d, J = 2.8 Hz, 1H), 7.04 (d, J = 4.8 Hz, 1H), 6.98−6.95 (m, 4H), 6.74 (d, J_{PH} = 4.4 Hz, 1H), 2.75 (t, J = 7.8 Hz, 2H), 2.22−2.06 (m, 2H), 1.61 (q, J = 7.4 Hz, 2H), 1.45 (m, 2H), 1.28−1.25 (m, 36 H), 0.89−0.83 (m, 6H). ^{31}P{^{1}H} NMR (162.0 MHz, $CO(CD_3)_2$): 27.7 (s), −143.0 (septet, J_{PF} = 708 Hz, PF_6). Anal. $C_{76}H_{85}F_{12}N_4S_5P_3Ru$ requires C, 55.77; H, 5.23; N, 3.42. Found: C, 55.38; H, 5.40; N, 3.31%.

[$Ru(bpy)_2PDo_2T_5$-*P*,*C*]PF_6 (9). To a deaerated solution of NaOH (12 g, 0.30 mol) dissolved in methanol (300 mL), **8** (1.00 g, 0.611 mmol) was added and the solution was heated to reflux. After 1 h, the solution turned from orange to a deep red. After being stirred at reflux for 16 h, the burgundy-red solution was condensed to 150 mL and pipetted dropwise into a solution of NH_4PF_6 (3.00 g, 17.3 mmol) in H_2O (200 mL) and stirred 1 h to give a red-black precipitate. Recrystallization from ethanol gave **9** as a very dark, red powder. Yield: 410 mg (45%). ^{1}H NMR (400.1 MHz, $CO(CD_3)_2$): δ 8.89 (d, J = 5.2 Hz, 1H), 8.63 (d, J = 8.0 Hz, 1H), 8.56 (d, J = 7.6 Hz, 1H), 8.48−8.44 (m, 3H), 8.12−8.08 (m, 1H), 8.00−7.89 (m, 4H), 7.77−7.72 (m, 2H), 7.66 (m, 1H), 7.50−7.43 (m, 5H), 7.37 (d, J = 5.2 Hz, 1H), 7.31 (t, J = 6.0 Hz, 1H), 7.19−7.13 (m, 3H), 7.06 (d, J = 4.0 Hz, 1H), 7.03 (d, J = 4.8 Hz, 1H), 6.98−6.92 (m, 3H), 6.86 (d, J = 5.2 Hz, 1H), 6.72 (d, J = 2.4 Hz, 1H), 6.54 (t, J = 8.0 Hz, 2H), 6.44 (s, 1H), 2.77 (m, 2H), 2.45 (m, 2H), 1.63 (m, 2H), 1.44 (m, 2H), 1.26 (m, 36 H), 0.84 (m, 6H). ^{31}P{^{1}H} NMR (162.0 MHz, $CO(CD_3)_2$): d 44.8 (s), −143.0 (septet, J_{PF} = 708 Hz, PF_6). Anal. $C_{76}H_{84}F_6N_4S_5P_2Ru$ requires C, 60.98; H, 5.66; N, 3.74. Found: C, 61.29; H, 5.78; N, 4.00%.

3,3‴′-Didodecyl-2,2′:5′,2″:5″,2‴:5‴,2⁗-pentathiophene (Do_2T_5, 10). A solution of IDo_2T_5 (300 mg, 0.343 mmol) in diethyl ether (100 mL) was cooled to −20 °C, and *n*-BuLi (0.26 mL, 1.6 M in hexanes, 0.41 mmol) was added. The yellow-orange solution immediately changed color to dark orange. H_2O (0.10 mL, 5.55 mmol) was injected into the solution, and with slow warming after 0.5 h, the solution turned yellow. The ether solution was washed three times with H_2O, dried with $MgSO_4$, and filtered, and the solvent was removed to leave a yellow residue. Purification by column chromatography on silica gel with hexanes gave **10** as a dark-yellow powder after removal of solvent. Yield: 257 mg (100%). ^{1}H NMR (400.1 MHz, $CDCl_3$): δ 7.17 (d, J = 5.2 Hz, 2H), 7.11 (d, J = 3.6 Hz, 2H), 7.08 (s, 2H), 7.01 (d, J = 3.6 Hz, 2H), 6.93 (d, J = 5.2 Hz, 2H), 2.77 (t, J = 7.8 Hz, 4H), 1.64 (m, 4H), 1.37−1.25 (m, 36 H), 0.87 (t, J = 6.6 Hz, 6H). Anal. $C_{44}H_{60}S_5$ requires C, 70.53; H, 8.07. Found: C, 70.93; H, 8.27%.

Acknowledgment. M.O.W. and C.B. thank the Natural Sciences and Engineering Research Council of Canada (NSERC) for support of this research. C.M. thanks NSERC and the University of British Columbia for Fellowship support. We thank Dr. Frank van Veggel, Peter Diamente, and Luis Netter for assistance with lifetime measurements.

Supporting Information Available: Selected bond lengths and angles for **1** and **4** and X-ray crystallographic files (CIF) for **3**, **6**, and **8**. $E_{op}/\Delta E$ correlation plots, solid-state UV−vis spectra and data, plots for lifetime measurements of **4** and **8**, and time-delayed luminescence spectra of **8**. This material is available free of charge via the Internet at http://pubs.acs.org.

JA043573A